

Spreading and Suppression of Infection Clusters on the Ginibre Continuum Percolation Clusters

Machiko Katori*

*Department of Mathematical Informatics,
Graduate School of Information Science and Technology,
The University of Tokyo, Hongo, Bunkyo-ku, Tokyo 113-0033, Japan*

Makoto Katori†

*Department of Physics, Faculty of Science and Engineering,
Chuo University, Kasuga, Bunkyo-ku, Tokyo 112-8551, Japan*

(Dated: June 30, 2021)

Abstract

Off-lattice SIR models are constructed on continuum percolation clusters defined on the Ginibre point process (GPP) and on the Poisson point process (PPP). The static percolation transitions in the continuum percolation models as well as the infection-spreading transitions in the SIR models, which are regarded as the dynamic percolation transitions, are enhanced in the GPP-based model compared with the PPP-based model. This enhancement is caused by hyperuniformity of the GPP. On the other hand, in the extinction phase of infection on the phase diagram, a wide parameter region is determined in which formation of infection clusters is suppressed in the GPP-based model compared with the PPP-based model. We think that the PPP approximates a disordered configuration of individuals and the GPP does a configuration of citizens adopting a strategy to keep social distancing in a city in order to avoid contagion. The suppression of infection clusters observed in the GPP-based model implies that such a strategy is effective when the infectivity is relatively small.

* katori-machiko@g.ecc.u-tokyo.ac.jp

† katori@phys.chuo-u.ac.jp

I. INTRODUCTION

In the previous paper [1], we introduced a new type of stochastic epidemic models defined on two-dimensional continuum percolation clusters. For the continuum percolation model known as the *standard Gilbert disk model* [2–4], we prepare a random configuration of points on \mathbb{R}^2 and put a set of disks with the same radius r centered at the points. When the distances of points are less than $2r$, the disks centered at these points overlap and form clumps of disks called *percolation clusters*. A statistical ensemble of random point configurations specified by a probability law is generally called a *point process* [5]. Here we assume that the point process has translational symmetry with a constant finite density ρ . The product of ρ and the area of a disk $a = \pi r^2$,

$$\kappa := \rho a = \rho \pi r^2, \tag{1}$$

is called the *filling factor*. A unique *critical value* κ_c is defined such that if $\kappa \leq \kappa_c$ any percolation cluster includes only finite number of disks with probability one, while if $\kappa > \kappa_c$ we have a positive probability $\Theta(\kappa) > 0$ to observe a percolation cluster involving an infinite number of disks an (*infinite percolation cluster*). We interpret each sample of point process as a realization of spatial configuration of individuals, and if and only if two disks overlap, then the individuals living at the centers of these disks are regarded as neighbors of each other. Infection can occur only between neighboring individuals, and hence our model is for a contagious disease. We introduce a parameter λ indicating *infectivity* so that each susceptible (S) individual will be infected with the rate λ multiplied by the total number of neighboring infected (I) individuals. And each I-individual becomes recovered (R) with a constant rate which is normalized to be unity. That is, we consider a SIR model with parameter λ on percolation clusters specified by a given point process with filling factor κ . When $\kappa > \kappa_c$, we can find an infinite percolation cluster with probability $\Theta(\kappa) > 0$ as mentioned above, and hence if we consider the SIR model on an infinite percolation cluster, we will see a phase transition at a critical infectivity $\lambda_c(\kappa)$ between an *extinction phase* ($\lambda \leq \lambda_c(\kappa)$) and an *infection-spreading phase* ($\lambda > \lambda_c(\kappa)$). In the former phase any infection process ceases with a finite duration of time with probability one, while in the latter phase processes can continue forever on an infinite percolation cluster with a positive probability $\Theta^{\text{SIR}}(\kappa, \lambda) > 0$. We notice that such *dynamical phase transitions* have been extensively studied for lattice SIR models [6–11] (or the lattice SIS models called the *contact processes*

[12–15]). The phase transitions in the lattice SIR models belong to the *dynamic percolation universality class* [6, 7, 16, 17]. The present epidemic models are off-lattice generalizations of the lattice SIR models.

For an underlying point process of our epidemic model, we have chosen the *Ginibre point process* (GPP) [18–20] which has been extensively studied in random matrix theory [21–23]. We compared infection processes on the GPP-based SIR model with those on the SIR model defined on the *Poisson point process* (PPP) [5]. While there is no correlation among points in the PPP, a repulsive interaction acts between any pair of points in the GPP and the system becomes *hyperuniform* [24, 25]. The hyperuniformity implies *rigidity* of the GPP in the sense that occasional appearance of clumping of points and vacant spaces are suppressed compared with the PPP [26]. As a result, a static percolation transition is enhanced in the GPP-based continuum percolation model than in the PPP-based model and hence we have an inequality

$$\kappa_c^{\text{GPP}} < \kappa_c^{\text{PPP}}. \quad (2)$$

Moreover, with a fixed κ_0 which was chosen to be greater than κ_c^{PPP} , we observed $\lambda_c^{\text{GPP}}(\kappa_0) < \lambda_c^{\text{PPP}}(\kappa_0)$, which means an enhancement of the dynamic percolation transition to the infection-spreading phase in the GPP-based SIR model compared with the PPP-based model [1].

At the same time, we studied infection processes with relatively small values of infectivity $\lambda < \lambda_c^{\text{GPP}}(\kappa_0)$ and found a parameter regime $0 < \lambda < \lambda_*(\kappa_0)$ in which formation of infection clusters are suppressed in the GPP-based SIR model compared with the PPP-based model. We think that the PPP approximates a disordered configuration of individuals and the GPP does a configuration of citizens adopting a strategy to keep social distancing in a city in order to avoid contagion. The above results seem to prove effectiveness of such a strategy at least in the time periods between epidemic waves of a contagious disease [1].

We have developed our numerical study on these new types of epidemic models and evaluated the critical values $\lambda_c(\kappa)$ and $\lambda_*(\kappa)$ by systematically changing the filling factor κ . In Fig. 1, the estimated phase boundaries between the extinction phases and the infection-spreading phases, $\lambda = \lambda_c^{\text{GPP}}(\kappa)$ and $\lambda = \lambda_c^{\text{PPP}}(\kappa)$, are plotted. Both of $\lambda_c^{\text{GPP}}(\kappa)$ and $\lambda_c^{\text{PPP}}(\kappa)$ are decreasing in κ so that for $\sharp = \text{GPP}$ and PPP , $\lambda_c^\sharp(\kappa) \rightarrow \infty$ as κ is approaching κ_c^\sharp from

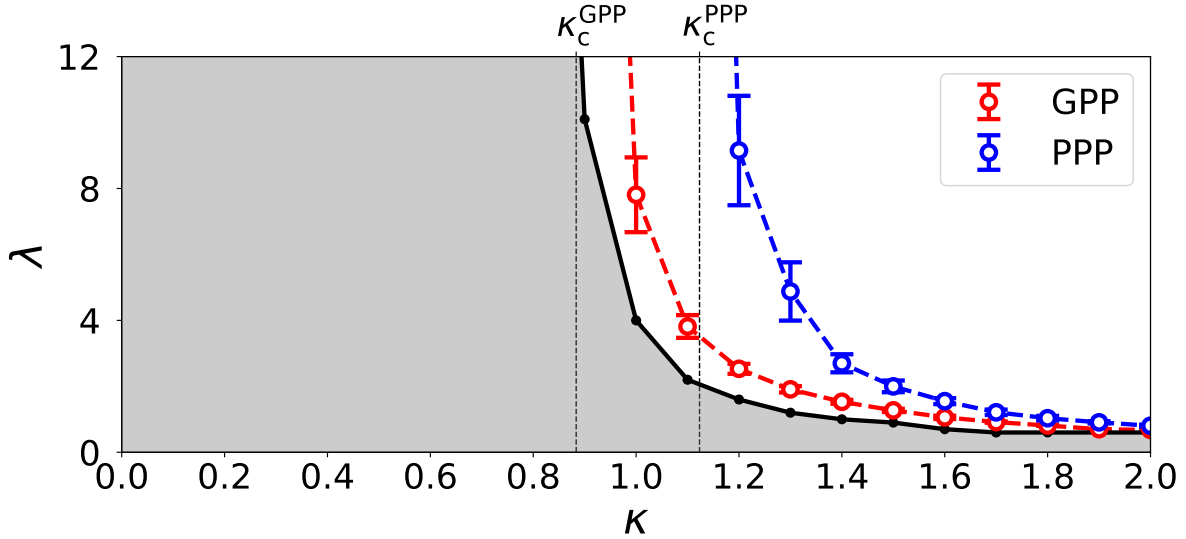


FIG. 1. Phase diagram of the present epidemic models estimated by numerical simulations. The phase boundaries between the extinction phases and the infection-spreading phases are shown by a red curve for the GPP-based SIR model and by a blue curve for the PPP-based model, respectively. The values of critical filling factors of continuum percolation transitions are indicated by vertical dotted lines, which are evaluated as $\kappa_c^{\text{GPP}} \simeq 0.884$ and $\kappa_c^{\text{PPP}} \simeq 1.12$. In the shaded region, infection clusters are suppressed in the GPP-based SIR model compared with the PPP-based model.

the above, $\lambda_c^\sharp(\kappa) \rightarrow 0$ as $\kappa \rightarrow \infty$, and the following inequality holds,

$$\lambda_c^{\text{GPP}}(\kappa) < \lambda_c^{\text{PPP}}(\kappa), \quad \kappa > \kappa_c^{\text{PPP}}. \quad (3)$$

In the extinction phase of infection, we have focused on the largest, but finite percolation cluster realized in our simulation and observed infection processes on it, each of which starts from a single infected individual. We define the mass of infection cluster as the total number of R-individuals in the final configuration of each process. Since this is equal to the cumulative number of I-individuals during a process, we write it as \mathcal{N}_I . We numerically obtained statistical average $\langle \mathcal{N}_I \rangle$, which is a function of κ and λ . Figure 2 shows the dependence of $\langle \mathcal{N}_I^{\text{GPP}} \rangle$ and $\langle \mathcal{N}_I^{\text{PPP}} \rangle$ on λ when $\kappa = 1.0$. We find an intersection of the two curves at $\lambda_*(\kappa = 1.0) \simeq 4.0$ and it implies that, if $\lambda < \lambda_*(1.0)$, formation of infection clusters is suppressed in the GPP-based SIR model compared with the PPP-based model. The parameter regime in which infection clusters are suppressed in the GPP-based SIR

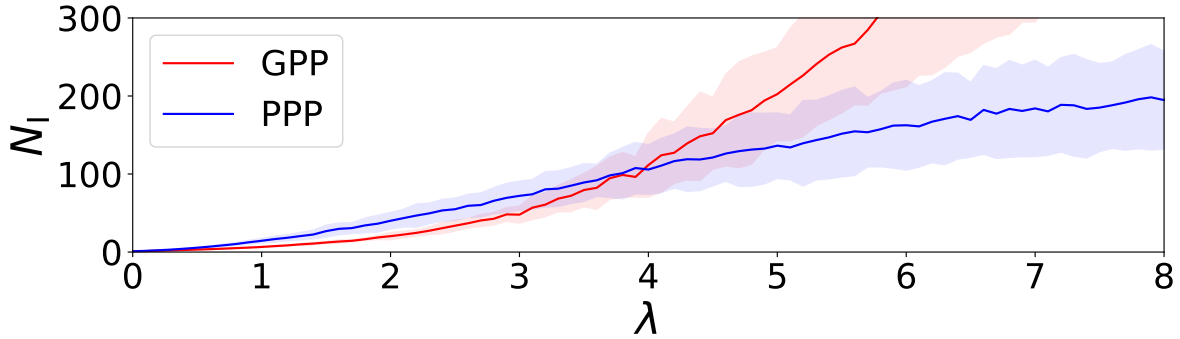


FIG. 2. Dependence on λ of masses of infection clusters in the extinction phase is shown for the two types of models with $\kappa = 1.0$. The solid curves show the means $\langle \mathcal{N}_I \rangle$ of 10 samples of underlying percolation clusters and the shaded strips do the standard deviations of them. The two curves intersect at $\lambda_* \simeq 4.0$, which implies that, if $\lambda < \lambda_*$ formation of infection clusters is suppressed in the GPP-based SIR model compared with the PPP-based model. The curve $\lambda = \lambda_*(\kappa)$, $\kappa > \kappa_c^{\text{GPP}}$ gives the right boundary of the shaded region in Fig. 1.

model is shown by the shaded region in Fig. 1.

II. THE GINIBRE AND THE POISSON CONTINUUM PERCOLATION MODELS

Let $N \in \{1, 2, \dots\}$. We prepared $2N \times 2N$ random matrices such that the real and the imaginary parts of each entry are independently and identically distributed real standard Gaussian random variables. Then we calculated $2N$ complex eigenvalues and plot them on the complex plane \mathbb{C} which is identified with the two-dimensional plane \mathbb{R}^2 . We have confirmed that almost all eigenvalues are uniformly distributed in a disk around the origin with radius $\sqrt{2N}$; that is, they follows the *circle law* [21, 22]. We have used only the point distribution in the central $\sqrt{\pi N} \times \sqrt{\pi N}$ square and performed a scale change by factor $1/\sqrt{\pi N}$ to obtain a point process on the unit square $[0, 1]^2$. The obtained point process has density $\rho_N^{\text{GPP}} = N$, which well approximates the GPP and is denoted by Ξ_N^{GPP} . The PPP is a uniform point process without any correlation and hence it is easy to generate samples of the PPP with N points in $[0, 1]^2$. The obtained point process is denoted by Ξ_N^{PPP} which has density $\rho_N^{\text{PPP}} = N$. For each sample of point process Ξ_N on $[0, 1]^2$, we imposed the periodic

boundary condition.

Consider a point process Ξ extended over whole \mathbb{R}^2 , which is a set of an infinite number of points with a finite constant density ρ . Then we introduce a real number $r > 0$. We place disks of radius r centered at each point; $B_r(x) := \{z \in \mathbb{R}^2 : |z - x| < r\}$, $x \in \Xi$. Two points $x \in \Xi$ and $y \in \Xi$ are neighbors, if and only if $B_r(x) \cap B_r(y) \neq \emptyset$. If there is a finite sequence of points $x_0, x_1, \dots, x_n \in \Xi$ such that $x_0 = x, x_n = y$ and x_{j+1} is a neighbor of x_j , $j = 0, 1, \dots, n - 1$, then the two points x and y are *connected*. The maximal connected components are called *percolation clusters* whose sizes are given by the numbers of points of Ξ included in the clusters. The above defines the *standard Gilbert disk model* with radius r , which is one of the *Boolean percolation models*, on the point process Ξ [2–4, 27–29]. It is said that the system percolates if there is at least one *infinite cluster*, whose size is infinity [30, 31]. It is proved that an infinite cluster exists uniquely with probability one for the Boolean percolation models on the PPP and the GPP [3, 4, 29]. The probability that the system percolates is called the *percolation probability*. In the present Boolean percolation model on \mathbb{R}^2 , it is a function of the filling factor κ defined by (1) [32]. We write the percolation probability as $\Theta(\kappa)$. There is a unique *critical value of filling factor* κ_c such that $\Theta(\kappa) = 0$ if $\kappa \leq \kappa_c$, and $\Theta(\kappa) > 0$ if $\kappa > \kappa_c$.

In the standard Gilbert disk model defined on a finite point process Ξ_N in $[0, 1]^2$, Θ is approximated by the ratio Θ_N of the number of points included in the largest cluster to the total number of points N [30]. We have generated 10 samples of finite approximations Ξ_N^{PPP} and Ξ_N^{GPP} for seven different N , $N = 1000, 2000, \dots, 7000$. In [1], we performed extrapolation of the numerical results to $N \rightarrow \infty$ and obtained the following evaluations,

$$\begin{aligned}\kappa_c^{\text{GPP}} &= 0.884 \pm 0.016, \\ \kappa_c^{\text{PPP}} &= 1.12 \pm 0.05.\end{aligned}\tag{4}$$

The above estimation of κ_c^{PPP} is consistent with the value reported in [32] evaluated using efficient algorithms [33–36], $\kappa_c^{\text{PPP}} = 1.12808737(6)$.

By the definition (1), κ denotes the total area of disks with radius r which are penetrable to each other. One of the origin of the difference of κ_c^{GPP} and κ_c^{PPP} shown above is the difference of frequencies of overlapping of disks under the same values of ρ and r in these two distinct point processes. Since the GPP is hyperuniform [24, 25], while the PPP is not, the overlapping of disks occurs less frequently in the GPP than in the PPP and hence

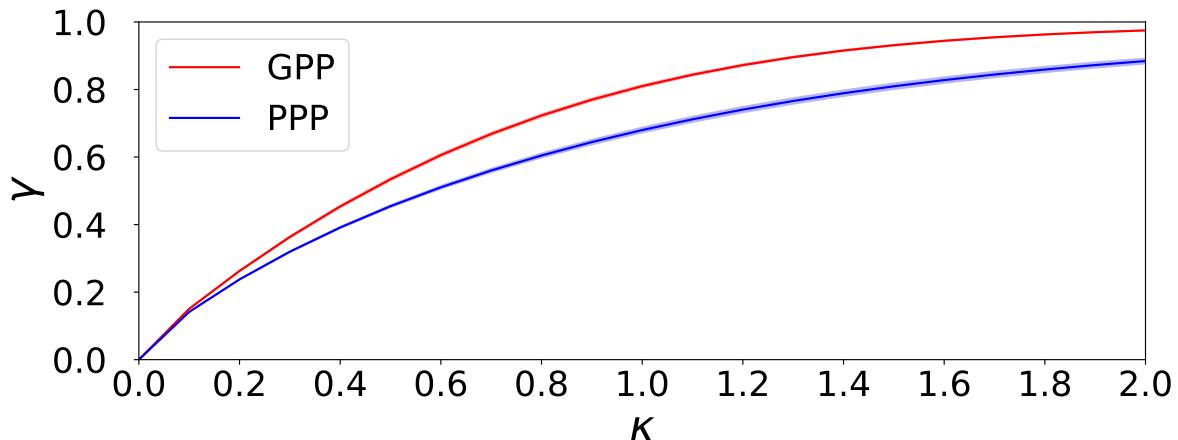


FIG. 3. Dependence on κ of the occupation ratios γ of the Ginibre disks and of the Poisson disks. Solid curves show the means of 10 samples and shaded strips do the standard deviations of them.

the *net area* of disks will be larger in the GPP than in the PPP under the same value of κ . Therefore, the percolation transition occurs on the GPP clusters at $\kappa = \kappa_c^{\text{GPP}}$ which is smaller than κ_c^{PPP} . Here we use the 10 samples with 1000 points on $[0, 1]^2$ for Ξ_{1000}^{GPP} and Ξ_{1000}^{PPP} , in which $\rho_N = N = 1000$. For each sample of random points on $[0, 1]^2$, we impose the periodic boundary condition and increase the radius r of disks centered at the points. At each value of $\kappa = \rho\pi r^2$, we measured the area a_{empty} of the subdomain in $[0, 1]^2$ which is *not* covered by any disk at all. We define the variable $\gamma := 1 - a_{\text{empty}} \in [0, 1]$, which indicates the net area of disks in the unit square, that is, $\gamma = |\bigcup_{x \in \Xi} B_r(x)|$. Figure 3 shows the occupation ratios of disks $\gamma = \gamma^\sharp(\kappa)$ for $\sharp = \text{GPP}$ and PPP . As expected $\gamma^{\text{GPP}}(\kappa) > \gamma^{\text{PPP}}(\kappa)$ for all $\kappa > 0$. By Fig. 3, the critical values of filling factor (4) are mapped to the following,

$$\begin{aligned} \gamma_c^{\text{GPP}} &= 0.763 \pm 0.005, \\ \gamma_c^{\text{PPP}} &= 0.719 \pm 0.008. \end{aligned} \tag{5}$$

If we interpret the site percolation model on the square lattice \mathbb{Z}^2 as the Bernoulli distribution of unit disks on sites with probability p , the percolation threshold $p_c \simeq 0.5927$ [30] will give the critical occupation ratio $\gamma_c^{\mathbb{Z}^2} = (\pi/4) \times p_c \simeq 0.4655$. The critical values (5) for the random point processes are greater than $\gamma_c^{\mathbb{Z}^2}$, which is due to the off-lattice effect. We see that the relative difference of κ_c 's, $|\kappa_c^{\text{GPP}} - \kappa_c^{\text{PPP}}|/(\kappa_c^{\text{GPP}} + \kappa_c^{\text{PPP}}) \simeq 0.12$ is reduced to $|\gamma_c^{\text{GPP}} - \gamma_c^{\text{PPP}}|/(\gamma_c^{\text{GPP}} + \gamma_c^{\text{PPP}}) \simeq 0.030$ for γ_c 's. It should be noticed that γ_c^{GPP} is larger than

γ_c^{PPP} . It suggests that even at the percolation threshold, overlapping of disks occurs less frequently in the GPP-based SIR model than in the PPP-based model. If we interpret centers of disks as locations of individuals, the above implies that the area per one individual in the GPP-based SIR model is larger than that in the PPP-based model. Hence if the infectivity λ is small enough, infection could be more suppressed in the GPP-based SIR model compared with in the PPP-based model.

III. SPREADING OF INFECTION ON CONTINUUM PERCOLATION CLUSTERS

For each finite approximation of point process Ξ_N on $[0, 1]^2$ with the periodic boundary condition, we have defined the continuum percolation model with the filling factor κ as explained above. Here we consider the supercritical case $\kappa > \kappa_c$. We pick up the largest percolation cluster and write it as \mathcal{G}_N . The size of \mathcal{G}_N is defined as the total number of disks included in it and denoted by $|\mathcal{G}_N|$. We use \mathcal{G}_N as an underlying graph of our contagious epidemic model of the SIR type as follows.

At each point $x \in \mathcal{G}_N$, we put a random variable $\eta(x) \in \{\text{S}, \text{I}, \text{R}\}$. We consider a continuous-time Markov process, $(\eta_t)_{t \geq 0}$, where $\eta_t := \{\eta_t(x) : x \in \mathcal{G}_N\}$. Let \mathbf{P}^η denote the probability in this Markov process starting from the configuration $\eta := \{\eta(x) : x \in \mathcal{G}_N\}$. The transition mechanism is given by

$$\begin{aligned} \mathbf{P}^\eta(\eta_t(x) = \text{I}, \eta(x) = \text{S}) &= \lambda c(x, \eta)t + o(t), \\ \mathbf{P}^\eta(\eta_t(x) = \text{R}, \eta(x) = \text{I}) &= t + o(t) \quad \text{as } t \rightarrow 0, \end{aligned} \tag{6}$$

where λ is a positive parameter called the infectivity and $c(x, \eta)$ is a positive function depending on a point x and a configuration η . That is, if an individual at point x is in the susceptible (S) state, it is infected (I) at rate $\lambda c(x, \eta)$, while if it is infected (I), it becomes recovered (R) at rate 1. Once $\eta(x) = \text{R}$, the state at x does not change forever. We require that only one-variable-change happens in each transition; that is, $\mathbf{P}^\eta(\eta_t(x) \neq \eta(x), \eta_t(y) \neq \eta(y)) = o(t)$ as $t \rightarrow 0$ for each $x, y \in \mathcal{G}_N$ with $x \neq y$ given a configuration η on \mathcal{G}_N [12, 13]. Here we set the function $c(x, \eta)$ as

$$c_{\text{linear}}(x, \eta) = \sum_{y: |y-x| < 2r} 1_{(\eta(y)=\text{I})}, \tag{7}$$

where $1_{(\omega)}$ is the indicator function of an event ω ; $1_{(\omega)} = 1$ if ω is satisfied and $1_{(\omega)} = 0$ otherwise. In other words, the infection rate is given by the total number of infected neighbors multiplied by the infectivity λ . In the previous paper [1], we called the SIR model with (7) the *linear model*. We have simulated this continuum Markov process on \mathcal{G}_N by the Gillespie algorithm [37–39]. This method is also called the n -fold way algorithm for spin systems [40].

If we consider the above SIR model on an *infinite* percolation cluster \mathcal{G} which is found in the supercritical phase $\kappa > \kappa_c$ formed on an infinite point process, we can discuss the percolation problem for an infection cluster consisting of I-individuals and R-individuals [6–17]. The percolation probability of infection cluster denoted by Θ^{SIR} is increasing in λ for each $\kappa > 0$ and a unique critical value $\lambda_c(\kappa)$, $\kappa > \kappa_c$, is defined so that

$$\begin{aligned}\Theta^{\text{SIR}}(\kappa, \lambda) &= 0, & \text{if } \lambda \leq \lambda_c(\kappa), \\ \Theta^{\text{SIR}}(\kappa, \lambda) &> 0, & \text{if } \lambda > \lambda_c(\kappa), \quad \text{for } \kappa > \kappa_c.\end{aligned}$$

In the present numerical simulation, we consider the off-lattice SIR model on a finite percolation cluster \mathcal{G}_N with $|\mathcal{G}_N| \leq N$. Therefore, any infection process on \mathcal{G}_N ceases sooner or later and in a final configuration we have a percolation cluster consisting of R-individuals embedded in a field of S-individuals. For each (κ, λ) , we simulated the SIR model from a single infected individual 100 times and evaluated the mean ratio of total number of R-individuals to $|\mathcal{G}_N|$ in a final configuration. We regard this as an approximation of infection probability $\Theta_N^{\text{SIR}}(\kappa, \lambda)$ with size N [6, 8, 9, 16]. Increasing the size N of point process Ξ_N systematically, we prepare a series of approximations $\{\Theta_N^{\text{SIR}}(\kappa, \lambda)\}_N$ with $N = 1000, 2000, 3000, 4000, 5000, 6000, \text{ and } 7000$.

We have evaluated $\lambda_c(\kappa)$ for $\kappa > \kappa_c$ by the following procedure. Fix $\kappa > \kappa_c$. For each $N = 1000, \dots, 7000$, we numerically generated 10 samples of Ξ_N and then \mathcal{G}_N , and have drawn curves Θ_N^{SIR} versus λ . For each curve an approximate value of critical infectivity denoted by $\lambda_c^{(N)}(\kappa)$ is defined by the value of λ at which the numerical value of $\partial\Theta_N^{\text{SIR}}(\kappa, \lambda)/\partial\lambda$ attains a maximum. We plot $\lambda_c^{\text{GPP}(N)}(\kappa)$ and $\lambda_c^{\text{PPP}(N)}(\kappa)$ versus $1/N$. Figure 4 shows the plots for $\kappa = 1.2$, where the error bars are estimated by the 10 samples for each N . The linear extrapolation with respect to $1/N$ gives $\lambda_c^{\text{GPP}}(1.2) = \lim_{N \rightarrow \infty} \lambda_c^{\text{GPP}(N)} = 2.53 \pm 0.15$, and $\lambda_c^{\text{PPP}}(1.2) = \lim_{N \rightarrow \infty} \lambda_c^{\text{PPP}(N)} = 9.15 \pm 1.66$. By this procedure the phase boundaries between the extinction phases and the infection-spreading phases of infection, $\lambda = \lambda_c^{\text{GPP}}(\kappa)$,

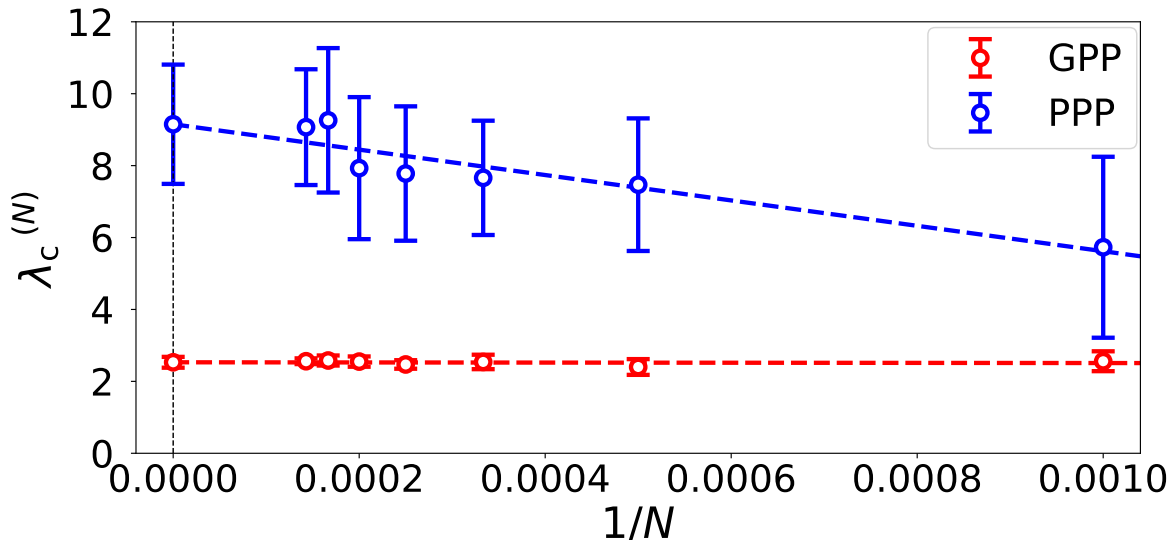


FIG. 4. Critical infectivities $\lambda_c^\sharp(\kappa)$ are evaluated for $\sharp = \text{GPP}$ and PPP by linear extrapolations of finite-size approximations $\lambda_c^{\sharp(N)}(\kappa)$ in the $1/N$ -plots. The case with $\kappa = 1.2$ is shown.

$\kappa > \kappa_c^{\text{GPP}}$, and $\lambda = \lambda_c^{\text{PPP}}(\kappa)$, $\kappa > \kappa_c^{\text{PPP}}$, are plotted in Fig. 1.

IV. SUPPRESSION OF INFECTION CLUSTERS IN THE GPP-BASED EPI-DEMIC MODEL

With $N = 1000$ we have prepared 10 samples of Ξ_N and then generate 10 finite percolation clusters \mathcal{G}_N with a filling factor $\kappa > 0$. Here we consider the extinction phase of infection, $\lambda < \lambda_c(\kappa)$. On each \mathcal{G}_N , we simulated the present off-lattice SIR model starting from a single infected individual 100 times. For each process of the SIR model with parameter λ , we counted the total number of R-individuals in the final configuration, which is equal to the cumulative number of I-individuals during the process and represents the mass of infection cluster. Then \mathcal{N}_I is defined as its mean value over the 100 runs of simulations. Moreover, we have averaged \mathcal{N}_I over 10 samples of \mathcal{G}_N to obtain $\langle \mathcal{N}_I \rangle$. Comparison of $\mathcal{N}_I^{\text{GPP}}$ and $\mathcal{N}_I^{\text{PPP}}$ was already demonstrated by Fig. 2 for $\kappa = 1.0$.

When $\kappa > \kappa_c^{\text{GPP}}$, we have found an intersection of the two curves $\langle \mathcal{N}_I^{\text{GPP}} \rangle = \langle \mathcal{N}_I^{\text{GPP}} \rangle(\lambda)$ and $\langle \mathcal{N}_I^{\text{PPP}} \rangle = \langle \mathcal{N}_I^{\text{PPP}} \rangle(\lambda)$ at $\lambda_*(\kappa)$. The value of $\lambda_*(\kappa)$ is decreasing in κ and behaves as $\lambda_*(\kappa) \rightarrow \infty$ as κ approaches κ_c^{GPP} from the above, and $\lambda_*(\kappa) \rightarrow 0$ as $\kappa \rightarrow \infty$. When

$\kappa \leq \kappa_c^{\text{GPP}}$, $\langle \mathcal{N}_I^{\text{GPP}} \rangle(\lambda) < \langle \mathcal{N}_I^{\text{PPP}} \rangle(\lambda)$ for any $\lambda > 0$ and there is no intersecting point. As shown by the shaded region in the κ - λ phase diagram of the epidemic models (Fig. 1), formation of infection clusters is suppressed in the GPP-based SIR model compared with the PPP-based model in the parameter regions (i) $\kappa \leq \kappa_c^{\text{GPP}}$ and (ii) $\lambda < \lambda_*(\kappa)$, $\kappa > \kappa_c^{\text{GPP}}$.

V. CONCLUDING REMARKS

We put three remarks on the present study.

(a) In the previous paper [1], we studied variations of the present off-lattice SIR model by modifying the function $c(x, \eta)$ specifying the infection transition (6). In particular, we reported that the suppression of infection clusters in the GPP-based SIR model is enhanced in the *quadratic mode*, in which $c(x, \eta)$ is given by

$$c_{\text{quad}}(x, \eta) = \left(\sum_{y: |y-x| < 2r} 1_{(\eta(y)=1)} \right)^2, \quad (8)$$

instead of (7). As reported in [1], the suppression of mass of infection clusters \mathcal{N}_I in the GPP-based SIR model is indeed enhanced in the quadratic model, but the value of $\lambda_*^{\text{quad}}(\kappa)$, $\kappa > \kappa_c^{\text{GPP}}$ does not change so much from $\lambda_*^{\text{linear}}(\kappa)$. See Fig. 5.

(b) For each $\kappa > \kappa_c$, we have a critical infectivity $\lambda_c(\kappa)$ for the present off-lattice SIR model. In the infection-spreading phase $\lambda > \lambda_c(\kappa)$, $\Theta^{\text{SIR}}(\kappa, \lambda)$ is positive and regarded as the *order parameter* of dynamic percolation transition. In the vicinity of the phase boundary, it is expected that $\Theta^{\text{SIR}}(\kappa, \lambda)$ behaves as

$$\Theta^{\text{SIR}}(\kappa, \lambda) \simeq \text{const.} (\lambda - \lambda_c(\kappa))^{\beta_{\text{SIR}}}, \quad \lambda \gtrsim \lambda_c(\kappa), \quad \kappa > \kappa_c, \quad (9)$$

with a critical exponent β_{SIR} . Such a power law indicates one of the critical phenomena. The present off-lattice SIR model will belong to the same universality class with the lattice SIR models, which is called the *dynamic percolation universality class*, and $\beta_{\text{SIR}} = 5/36$ [6–8, 16]. Using the simulation results on the largest systems with $N = 7000$, we applied the least-square linear regression to log-log plots of the data $\Theta_{7000}^{\text{SIR}}(\kappa, \lambda)$ versus $\lambda - \lambda_c(\kappa)$ for $\kappa > \kappa_c$, where $\lambda_c(\kappa)$ is regarded as a fitting parameter, while the slope of fitting line is fixed to be $5/36 = 0.1388 \dots$. Figure 6 shows the best fitting result when $\kappa = 1.3$, which gives $\lambda_c^{\text{GPP}}(1.3) \simeq 2.08$ and $\lambda_c^{\text{PPP}}(1.3) \simeq 4.60$. In Fig. 5 we plotted the values of $\lambda_c^{\#}(\kappa)$, $\# =$

GPP and PPP by this method. The results are consistent with those obtained by the linear extrapolation method $\lambda_c^\sharp(\kappa) = \lim_{N \rightarrow \infty} \lambda_c^{\sharp(N)}(\kappa)$ in the $1/N$ -plots explained in Section III. It means the validity of the assumption (9) with $\beta_{\text{SIR}} = 5/36$.

(c) While the original SIR model was given by a system of deterministic differential equations [41], the lattice SIR models include randomness and are described by stochastic processes [6–11]. In the present off-lattice versions, we have introduced another randomness to generate spatial configurations of individuals. It is an interesting problem to compare the lattice SIR models and the present off-lattice SIR models based on random point processes. As mentioned in the item (b), the additional randomness of underlying graphs seems to be irrelevant for the critical phenomena associated with the infection transitions at λ_c . The values of critical infectivity λ_c are, however, sensitive to the point configurations of individuals. For the triangular (T), the square (S), and the honeycomb (H) lattices in two dimensions, the filling factors (1) are calculated as $\kappa^{\text{T}} = \sqrt{3}\pi/6 = 0.906\dots$, $\kappa^{\text{S}} = \pi/4 = 0.785\dots$, and $\kappa^{\text{H}} = \sqrt{3}\pi/9 = 0.604\dots$, respectively. The critical infectivities were reported as $\lambda_c^{\text{T}} = 4.0068(2)$ [42], $\lambda_c^{\text{S}} = 4.66571(3)$ [9], and $\lambda_c^{\text{H}} = 6.179(5)$ [42], respectively. Recently Santos et al. [11] simulated the SIR model on the Penrose tiling and evaluated as $\lambda_c^{\text{P}} = (1 - 0.1713(2))/0.1713(2) = 4.838(7)$. We have the value $\kappa^{\text{P}} = \sqrt{2}(5 - \sqrt{5})^{1/2}\pi/10 = 0.738\dots$ [43]. As shown by Fig. 5, we see the tendency such that λ_c^b decreases as κ^b increases for $b = \text{H, P, S, T}$, which is in common with the critical lines $\lambda = \lambda_c^\sharp(\kappa)$, $\kappa < \kappa_c^\sharp$ for $\sharp = \text{GPP and PPP}$. Moreover, we notice an approximate reciprocal law $\lambda_c^b \simeq 3.66/\kappa^b$, $b = \text{H, P, S, T}$. The spatial configurations of individuals are deterministic in the lattice SIR models, random but having hyperuniformity in the GPP [24, 25], and uniformly random-distributed in PPP, respectively. Hence we say that, for each infectivity $\lambda > 0$, the spread of infection can be observed only in higher values of filling factor κ of individuals, as the randomness of spatial configuration of individuals is increased. Further systematic studies of the dependence of λ_c of the SIR models on the underlying graphs are required, in which deterministic but heterogeneous lattices [11], random point processes [1], as well as a variety of randomly perturbed lattices [44] shall be considered.

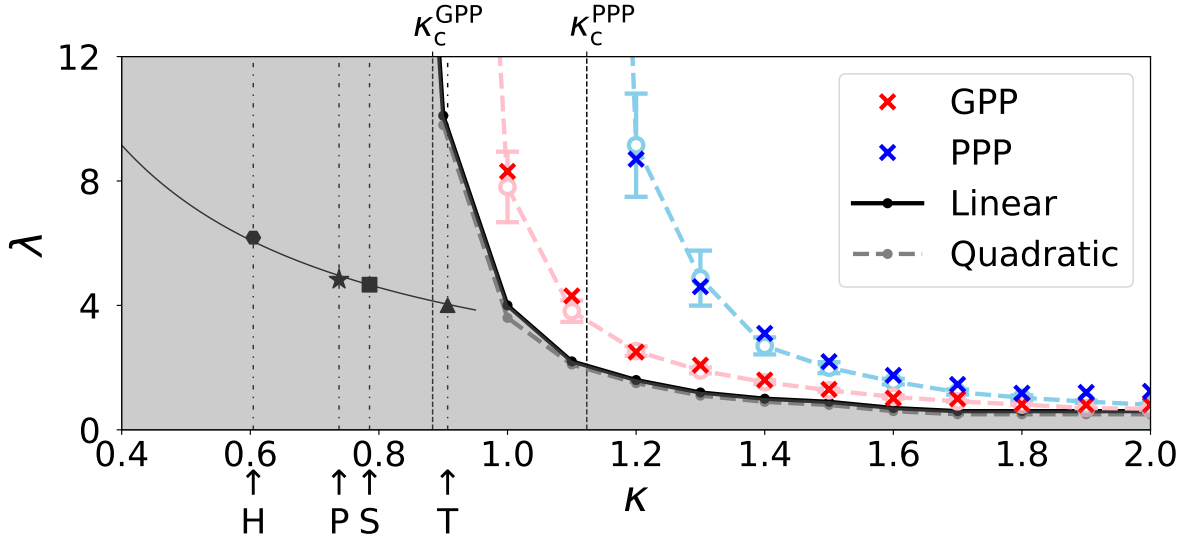


FIG. 5. (a) The values of $\lambda_*^{\text{quad}}(\kappa)$, $\kappa > \kappa_c^{\text{GPP}}$ of the quadratic model are superposed on the results of the linear model. The numerical difference of them is very small. (b) The critical infectivities $\lambda_c(\kappa)$ for $\kappa > \kappa_c$ evaluated using the power law (9) are dotted by red crosses (resp. blue crosses) for the GPP-based (resp. PPP-based) SIR models. The results are consistent with the phase boundaries determined by the $1/N$ -extrapolation method of finite-size approximations shown by light red and light blue. (c) The dependence of λ_c on κ is shown for the lattice SIR models on the triangular (T), the square (S), the Penrose (P), and the honeycomb (H) lattices, which is well approximated by $\lambda_c \simeq 3.66/\kappa$.

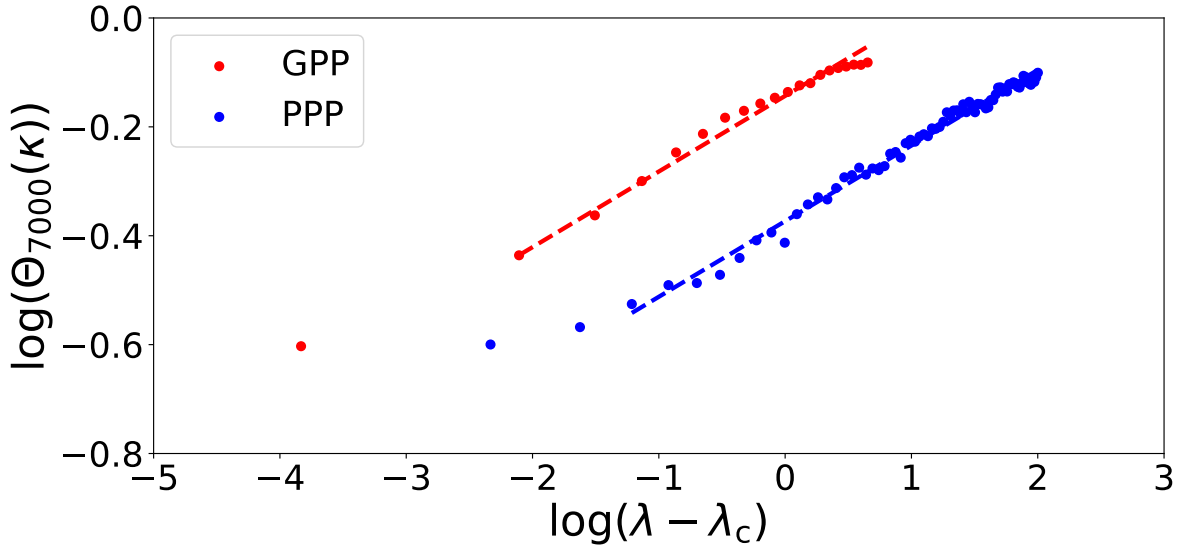


FIG. 6. The least-square linear regression was applied to the log-log plots of the data $\Theta_{7000}^{\text{SIR}}(\kappa = 1.3, \lambda)$ versus $\lambda - \lambda_c(1.3)$, where $\lambda_c(1.3)$ is a fitting parameter and the slope of fitting line is fixed to be $5/36 = 0.1388\dots$. The evaluated values are $\lambda_c^{\text{GPP}}(1.3) \simeq 2.08$ and $\lambda_c^{\text{PPP}}(1.3) \simeq 4.60$, respectively.

ACKNOWLEDGEMENTS

The present authors would like to thank Robert M. Ziff for allowing them to use the results reported in their preprint. They also thank Tomonari Dotera for useful discussion on quasicrystal lattices. Machiko K. thanks to T.J.Kobayashi for encouraging the present work. Makoto K. expresses his gratitude to John W. Essam for a stimulating communication which motivated this study. Machiko K. was supported by the ANRI Fellowship and International Graduate Program of Innovation for Intelligent World (IIW) of The University of Tokyo. Makoto K. was supported by the Grant-in-Aid for Scientific Research (C) (No.19K03674), (B) (No.18H01124), (S) (No.16H06338), and (A) (No.21H04432) of Japan Society for the Promotion of Science.

Machiko K. and Makoto K. designed and performed the research and the paper was

written cooperatively. Machiko K. performed computer simulations and data analysis.

- [1] Machiko Katori and Makoto Katori, *Phys. A Stat. Mech. its Appl.* , 126191 (2021), arXiv:2103.08461.
- [2] E. N. Gilbert, *J. Soc. Ind. Appl. Math.* **9**, 533 (1961).
- [3] R. Meester and R. Roy, *Continuum Percolation*, Cambridge Tracts in Mathematics (Cambridge University Press, Cambridge, 1996).
- [4] B. Bollobas and O. Riordan, *Percolation* (Cambridge University Press, Cambridge, 2006).
- [5] D. J. Daley and D. Vere-Jones, *An Introduction to the Theory of Point Processes*, 2nd ed., Probability and its Applications (Springer-Verlag, New York, 2003).
- [6] P. Grassberger, *Math. Biosci.* **63**, 157 (1983).
- [7] M. A. Muñoz, R. Dickman, A. Vespignani, and S. Zapperi, *Phys. Rev. E* **59**, 6175 (1999).
- [8] D. R. de Souza and T. Tomé, *Phys. A Stat. Mech. its Appl.* **389**, 1142 (2010).
- [9] T. Tomé and R. M. Ziff, *Phys. Rev. E* **82**, 051921 (2010).
- [10] S. Saha, A. Mishra, S. K. Dana, C. Hens, and N. Bairagi, *Phys. Rev. E* **102**, 052307 (2020).
- [11] G. Santos, T. Alves, G. Alves, A. Macedo-Filho, and R. Ferreira, *Phys. Lett. A* **384**, 126063 (2020).
- [12] T. M. Liggett, *Interacting Particle Systems*, Classics in Mathematics (Springer, Berlin, Heidelberg, 1985).
- [13] T. M. Liggett, *Stochastic Interacting Systems: Contact, Voter and Exclusion Processes*, Grundlehren der mathematischen Wissenschaften, Vol. 324 (Springer, Berlin, Heidelberg, 1999).
- [14] J. Marro and R. Dickman, *Nonequilibrium Phase Transitions in Lattice Models*, Collection Alea-Saclay: Monographs and Texts in Statistical Physics (Cambridge University Press, 1999).
- [15] H. Hinrichsen, *Adv. Phys.* **49**, 815 (2000).
- [16] J. L. Cardy and P. Grassberger, *J. Phys. A. Math. Gen.* **18**, L267 (1985).
- [17] R. M. Ziff, *Phys. A Stat. Mech. its Appl.* **568**, 125723 (2021).
- [18] J. Ginibre, *J. Math. Phys.* **6**, 440 (1965).
- [19] T. Shirai, *J. Stat. Phys.* **123**, 615 (2006).
- [20] J. Hough, M. Krishnapur, Y. Peres, and B. Virág, *Zeros of Gaussian Analytic Functions and*

- Determinantal Point Processes*, University Lecture Series, Vol. 51 (American Mathematical Society, Providence, Rhode Island, 2009).
- [21] M. L. Mehta, *Random Matrices*, 3rd ed. (Elsevier, Amsterdam, 2004).
- [22] P. J. Forrester, *Log-Gases and Random Matrices (LMS-34)* (Princeton University Press, Princeton, 2010).
- [23] M. Katori, *Bessel Processes, Schramm–Loewner Evolution, and the Dyson Model*, Springer-Briefs in Mathematical Physics, Vol. 11 (Springer, Singapore, 2016).
- [24] S. Torquato, Phys. Rep. **745**, 1 (2018).
- [25] T. Matsui, M. Katori, and T. Shirai, J. Phys. A Math. Theor. **54**, 165201 (2021).
- [26] S. Ghosh and J. L. Lebowitz, Indian J. Pure Appl. Math. **48**, 609 (2017).
- [27] B. Błaszczyszyn and D. Yogeshwaran, Electron. J. Probab. **18**, 1 (2013), arXiv:1112.2227.
- [28] B. Błaszczyszyn and D. Yogeshwaran, Adv. Appl. Probab. **46**, 1 (2014), arXiv:1111.6017.
- [29] S. Ghosh, M. Krishnapur, and Y. Peres, Ann. Probab. **44**, 3357 (2016).
- [30] D. Stauffer and A. Aharony, *Introduction To Percolation Theory* (Taylor & Francis, London, 1992).
- [31] J. W. Essam, Discrete Math. **1**, 83 (1971).
- [32] S. Mertens and C. Moore, Phys. Rev. E **86**, 061109 (2012), arXiv:1209.4936.
- [33] J. Quintanilla and S. Torquato, J. Chem. Phys. **111**, 5947 (1999).
- [34] J. Quintanilla, S. Torquato, and R. M. Ziff, J. Phys. A. Math. Gen. **33**, L399 (2000).
- [35] M. E. J. Newman and R. M. Ziff, Phys. Rev. E **64**, 016706 (2001), arXiv:0101295 [cond-mat].
- [36] J. A. Quintanilla and R. M. Ziff, Phys. Rev. E **76**, 051115 (2007).
- [37] D. T. Gillespie, J. Comput. Phys. **22**, 403 (1976).
- [38] D. T. Gillespie, J. Phys. Chem. **81**, 2340 (1977).
- [39] R. Erban and S. J. Chapman, *Stochastic Modelling of Reaction–Diffusion Processes*, Cambridge Texts in Applied Mathematics (Cambridge University Press, 2020).
- [40] A. B. Bortz, M. H. Kalos, and J. L. Lebowitz, J. Comput. Phys. **17**, 10 (1975).
- [41] W. O. Kermack and A. G. McKendrick, Proc. R. Soc. London. Ser. A, Contain. Pap. a Math. Phys. Character **115**, 700 (1927).
- [42] T. Tomé, D. R. de Souza, and R. M. Ziff, preprint (2013).
- [43] C. L. Henley, Phys. Rev. B **34**, 797 (1986).
- [44] S. Ghosh, N. Miyoshi, and T. Shirai, arXiv (2020), arXiv:2009.08811.